Manufacturing Letters 32 (2022) 32–38

Contents lists available at ScienceDirect

Manufacturing Letters

journal homepage: www.elsevier.com/locate/mfglet

Letters

Bayesian optimization for inverse calibration of expensive computer models: A case study for Johnson-Cook model in machining ☆

Jaydeep Karandikar [a,*], Anirban Chaudhuri [b], Timothy No [c], Scott Smith [a], Tony Schmitz [a,c]

[a] Oak Ridge National Laboratory, Oak Ridge, TN, USA
[b] University of Texas at Austin, Austin, TX 78712, USA
[c] University of Tennessee at Knoxville, Knoxville, TN 37996, USA

ARTICLE INFO

Article history:
Received 20 September 2021
Received in revised form 6 January 2022
Accepted 16 February 2022
Available online 4 March 2022

Keywords:
Inverse model calibration
Bayesian optimization
Machining
Finite element model calibration
Bounded objective function

ABSTRACT

Inverse model calibration for identifying the constitutive model parameters can be computationally demanding for expensive-to-evaluate simulation models. This paper presents a modified Bayesian optimization (BO) method, denoted as BO-bound, that incorporates theoretical bounds on the quantity of interest. A case study for the inverse calibration of the Johnson Cook (J-C) flow stress model parameters is presented using machining (cutting) force data. The results show fast calibration of the five J-C parameters within 25 simulations. In general, the BO-bound method is applicable for inverse calibration of any expensive simulation models as well as optimization problems with known bounds.

Published by Elsevier Ltd on behalf of Society of Manufacturing Engineers (SME).

1. Introduction

Finite element (FE) methods are widely used for modeling complex manufacturing processes. However, FE methods require a new constitutive model for each material system to describe its behavior (e.g., flow stress behavior during the shearing action in metal cutting). The constitutive model parameters can be determined through direct methods that employ high strain rate/temperature testing to measure the behavior or by inverse methods that use manufacturing process data to infer the parameters. For complex constitutive models with many parameters, the inverse method is preferred [1–3]. The inverse method finds the optimal parameter set that minimizes the difference between the predicted process variables, such as force and temperature, from the FE model and the experimental values from the manufacturing tests; this is done by iteratively modifying the model parameters for each FE simulation [2]. The methods described in the literature for inverse calibration of the constitutive model parameters in manufacturing use gradient-based methods, evolutionary algorithms, or hybrid approaches [2]. A major limitation of the existing methods is the relatively large number of simulations required for inverse calibration, especially when the gradient information is not readily available. This can make the methods computationally prohibitive for expensive-to-evaluate FE models, which can take many hours to complete. To address this challenge, this paper presents a Bayesian optimization (BO) method [4–7] that accounts for the bounded nature of the error functions used in deterministic inverse calibration of the constitutive model parameters.

In this work, the inverse calibration of the Johnson–Cook (J-C) model [1] is used as a case-study. The J-C model is widely-used in the machining community for modeling material flow stress behavior in machining operations. Note that, in general, the described BO approach can be used for calibrating any other model and manufacturing process. The J-C model empirically describes the material flow stress as a function of the strain, strain rate, and temperature as

$$\text{flowstress} = [A + B\epsilon^n]\left[1 + C\ln\left(\frac{\dot{\epsilon}}{\dot{\epsilon}_0}\right)\right]\left[1 - \left(\frac{T_{\text{mat}} - T_{\text{ref}}}{T_{\text{melt}} - T_{\text{ref}}}\right)^m\right], \quad (1)$$

where ϵ is the plastic strain, $\dot{\epsilon}$ is the plastic strain rate, $\dot{\epsilon}_0$ is the reference strain rate, T_{mat} is the material temperature, T_{ref} is the reference temperature at or below which there is no temperature

☆ This manuscript has been authored in part by UT-Battelle, LLC, under contract DE-AC05-00OR22725 with the US Department of Energy (DOE). The US government retains and the publisher, by accepting the article for publication, acknowledges that the US government retains a nonexclusive, paid-up, irrevocable, worldwide license to publish or reproduce the published form of this manuscript, or allow others to do so, for US government purposes. DOE will provide public access to these results of federally sponsored research in accordance with the DOE Public Access Plan (http://energy.gov/downloads/doe-public-access-plan).

* Corresponding author.
E-mail address: karandikarjm@ornl.gov (J. Karandikar).

https://doi.org/10.1016/j.mfglet.2022.02.001
2213-8463/Published by Elsevier Ltd on behalf of Society of Manufacturing Engineers (SME).

dependence of the yield stress, and T_{melt} is the material melting temperature. The J-C model parameters are the yield strength of the material under reference conditions A, the strain hardening constant B, the strain rate strengthening coefficient C, the strain hardening coefficient n, and the thermal softening coefficient m. Direct calibration of the J-C model parameters for machining with tension/compression split-Hopkinson pressure bar tests is difficult due to the high strains, strain rates, and temperatures [8–11].

There have been various methods presented in the literature for inverse calibration of J-C model parameters. These include iterative gradient-based search methods [12,13], response surface methodology [14], evolutionary algorithms such as particle swarm and genetic algorithms [15–17], and Bayesian calibration [8]. This work focuses on deterministic inverse model calibration using BO, which is a derivative-free global optimizer [4,5]. Gradient-based methods can also be used for efficient local optimization when adjoints are available. In absence of adjoints (e.g., when using commercial/proprietary FE software), gradients estimated through finite difference can result in a computationally challenging number of expensive simulations. The global BO is computationally comparable to local gradient-based solvers when adjoints are available and can be more efficient in the absence of adjoints for low to medium dimensional problems. The objective function in BO is approximated using a Gaussian process (GP) regression surrogate that provides the prediction mean and the prediction uncertainty. The GP surrogate is refined sequentially using an acquisition function to make the optimal sampling decisions in every iteration that contribute towards converging to the global optimum. The expected improvement (EI) is the most popular acquisition function [4,6]. In this work, the normalized mean absolute error (NMAE) between the experimental and the simulated process variables is used as the objective for model calibration, which has a theoretical lower bound of zero. However, the generic EI function does not account for the bounded nature of objective functions encountered in the inverse calibration problems and this limitation is addressed here.

The two primary contributions of the paper are: (1) the BO-bound method, which is a BO method that incorporates the theoretical bounds in the underlying quantity of interest; and (2) the application of the BO-bound method to the inverse calibration of expensive computer models using NMAE as the objective function. To address the limitation of the EI acquisition function in BO not accounting for bounds, a closed-form expression for EI was derived for the BO-bound method that can incorporate the theoretical bounds of the objective function. Note that the described BO-bound method can be used for any optimization problem where there exists a known bound (upper or lower) on the objective function. An alternate application could be the optimization of process parameters in laser additive manufacturing to minimize part porosity, where the part porosity has a lower bound of zero.

The remainder of the paper is organized as follows. Section 2 gives an overview of the standard BO method and describes the proposed BO-bound method that incorporates the NMAE lower bound of zero. Section 3 presents results for inverse calibration of the J-C flow stress model parameters for machining and a comparison of the BO-bound method with the standard BO method. Section 4 presents conclusions and future work.

2. Bayesian optimization for inverse calibration of J-C model parameters

The inverse calibration problem for identifying the J-C model parameters by minimizing the NMAE between the simulated and experimental observations is detailed in Section 2.1. The standard BO method for inverse calibration is then presented in Section 2.2. Finally, the proposed BO-bound method that incorporates the non-negative property of the NMAE is described in Section 2.3.

2.1. Inverse calibration problem setup

For a given set of parameters specific to a workpiece material and tool geometry (such as rake angle and rake face shape), FE simulation can be used to predict the tangential component of the cutting force, $F_{\text{T}}^{\text{sim}}$, which is aligned with the cutting speed direction, and the normal component of the cutting force, $F_{\text{N}}^{\text{sim}}$, which is perpendicular to the machined surface. In this case, the inputs to the system are the five J-C parameters $\mathbf{x} := \{A, B, C, n, m\} \in \mathscr{X} \subseteq \mathbb{R}^5$, where $\mathscr{X}$ denotes the parameter search space. The system output is denoted by $y = f(\mathbf{x})$, where $f : \mathscr{X} \mapsto \Omega \subseteq \mathbb{R}$, which is the NMAE between the experimental and simulated tangential and normal force components obtained through the expensive FE model simulation at $\mathbf{x}$ as given by

$$f(\mathbf{x}) := \text{NMAE}(A, B, C, n, m) = \frac{1}{2}\left(\frac{|F_{\text{T}}^{\text{sim}}(\mathbf{x}) - F_{\text{T}}^{\text{expt}}|}{F_{\text{T}}^{\text{expt}}} + \frac{|F_{\text{N}}^{\text{sim}}(\mathbf{x}) - F_{\text{N}}^{\text{expt}}|}{F_{\text{N}}^{\text{expt}}}\right). \tag{2}$$

The superscript sim denotes results from the FE model and the superscript expt denotes the experimental results. The optimization problem is defined as $\mathbf{x}^* = \arg\min_{\mathbf{x}\in\mathscr{X}} f(\mathbf{x})$. Although minimizing the NMAE results in non-unique solutions for the J-C model parameters, each solution is considered valid for the goal of accurately predicting the cutting force components through FE simulations [1,8,9].

2.2. BO for inverse calibration of expensive functions

BO is a GP-based method for sequentially converging to the global optimum. Given k samples of the NMAE, the next sampling location $\mathbf{x}_{k+1}$ to simulate and update the GP surrogate is selected by maximizing an acquisition function, $J(\mathbf{x})$, as $\mathbf{x}_{k+1} = \arg\max_{\mathbf{x}\in\mathscr{X}} J(\mathbf{x})$.

EI is the most popular acquisition function and uses the expected value of improvement to balance trade-offs between exploration (global search) and exploitation (local search) [4,6]. For a minimization problem, the improvement function $I(\mathbf{x})$ at any $\mathbf{x}$ is defined based on improving beyond the current observed best solution y_{min}^k after k sample evaluations as

$$I(\mathbf{x}) := \begin{cases} y_{\text{min}}^k - \mathscr{Y}(\mathbf{x}), & \mathscr{Y}(\mathbf{x}) \leqslant y_{\text{min}}^k \\ 0, & \mathscr{Y}(\mathbf{x}) > y_{\text{min}}^k, \end{cases} \tag{3}$$

where $\mathscr{Y}(\mathbf{x}) \sim \mathcal{N}(\mu(\mathbf{x}), \sigma(\mathbf{x}))$ is the GP prediction at any $\mathbf{x}$ with $\mu(\mathbf{x})$ denoting the GP prediction mean and $\sigma(\mathbf{x})$) denoting the GP prediction standard deviation that gives a measure of uncertainty in the prediction. The EI acquisition function at any given $\mathbf{x}$ is [4]

$$\mathbb{E}[I(\mathbf{x})] = \big(y_{\text{min}}^k - \mu(\mathbf{x})\big)\Phi(\beta(\mathbf{x})) + \sigma(\mathbf{x})\phi(\beta(\mathbf{x})), \tag{4}$$

where $\mathbb{E}$ denotes expectation, $\beta(\mathbf{x}) = \big(y_{\text{min}}^k - \mu(\mathbf{x})\big)/\sigma(\mathbf{x})$, $\Phi(.)$ is the standard normal cumulative distribution function, and $\phi(.)$ is the standard normal probability density function (see A.1 for derivation and a demonstration in Example 1).

2.3. BO-bound for inverse calibration of expensive functions with theoretical bounds

For the inverse calibration problem, the lower bound for NMAE is known to be zero. The GP surrogate is data-driven and cannot directly incorporate the underlying theoretical bounds on the quantity of interest. As a result, the GP can predict negative values for NMAE, which are unattainable. Within the standard BO framework, the incorrect negative NMAE predictions from the GP surrogate are propagated to the EI acquisition function, which could lead

to a misinformed choice of the sampling location. In this work, the objective function theoretical bounds are incorporated within the BO framework by redefining the improvement function. The modified improvement function $I_B(\mathbf{x})$ restricts the maximum predicted improvement to be $y^k_{\min}$ as

$$I_B(\mathbf{x}) := \begin{cases} y^k_{\min}, & \mathscr{Y}(\mathbf{x}) \leqslant 0 \\ y^k_{\min} - \mathscr{Y}(\mathbf{x}), & 0 < \mathscr{Y}(\mathbf{x}) \leqslant y^k_{\min} \\ 0, & \mathscr{Y}(\mathbf{x}) > y^k_{\min}, \end{cases} \tag{5}$$

When $\mathscr{Y}(\mathbf{x}) \leqslant 0$, the maximum improvement is restricted to $y^k_{\min}$ by suppressing the GP prediction to zero when predicted to be negative. Note that $I_B(\mathbf{x})$ can be similarly defined for any given bounds on the objective function making the BO-bound method applicable to other cases beyond the inverse calibration problem.

The modified EI at any given x can be derived in closed-form (see A.2 for derivation) as

$$\begin{aligned} \mathbb{E}[I_B(\mathbf{x})] = \Phi(\alpha(\mathbf{x}))y^k_{\min} + (y^k_{\min} - \mu(\mathbf{x}))(\Phi(\beta(\mathbf{x})) - \Phi(\alpha(\mathbf{x}))) \\ + \sigma(\mathbf{x})(\phi(\beta(\mathbf{x})) - \phi(\alpha(\mathbf{x}))), \end{aligned} \tag{6}$$

where $\alpha(\mathbf{x}) = (0 - \mu(\mathbf{x}))/\sigma(\mathbf{x})$. The BO method with the modified EI function for objective functions with theoretical bounds is denoted as BO-bound. Appendix A provides a comparison between the EI values in standard BO and BO-bound through Example 1.

Algorithm 1: BO/BO-bound pseudo-code

Input: Number of initial samples k_{init}, total number of simulations k_{total}, NMAE simulation model $f(.)$
Output: Optimal J-C parameters $\mathbf{x}^*$, optimal NMAE $f(\mathbf{x}^*)$
1: Initial Latin hypercube sampling (LHS) of k_{init} points
2: Determine the force values, $F_{\text{T}}^{\text{sim}}$ and $F_{\text{N}}^{\text{sim}}$ by FE simulation and the corresponding NMAE values $\{f(\mathbf{x}_i)\}_{i=1}^{k}$ using Eq. (2)
3: $k = k_{\text{init}}$
4: **while** $k \leqslant k_{\text{total}}$ **do**
5: Fit GP surrogate to the available training data $\{\mathbf{x}_i, f(\mathbf{x}_i)\}_{i=1}^{k}$
6: Select next sample $\mathbf{x}_{k+1}$ that maximizes the acquisition function in Eq. (4) for BO or Eq. (6) for BO-bound
7: Run FE simulation at the selected sample $\mathbf{x}_{k+1}$ and determine NMAE value $f(\mathbf{x}_{k+1})$ using Eq. (2)
8: $k = k + 1$
9: **end while**
10: Find optimal parameters $\mathbf{x}^* = \arg\min \{f(\mathbf{x}_i)\}_{i=1}^{k}$ ▷Optimal NMAE is given by $f(\mathbf{x}^*)$
11: **return** $\mathbf{x}^*, f(\mathbf{x}^*)$

3. Results

The BO-bound method was evaluated using an experimental result for orthogonal (or two-dimensional) turning reported in [8]. The material was Aluminum 6061-T6. The cutting tool had a rake angle of 15° and a relief angle of 8°. The cutting speed was 60 m/min, the feed was 0.3 mm/rev, and the depth of cut was 1 mm. The tangential cutting force component $F_{\text{T}}^{\text{expt}}$ was 224.1 N and normal cutting force component $F_{\text{N}}^{\text{expt}}$ was 95.1 N. The proposed BO-bound method was first compared with the standard BO method by fixing three of the five J-C parameters to illustrate the efficiency and robustness of the method. Subsequently, BO-bound method was applied for the inverse calibration of all five J-C parameters using expensive FE simulations. The procedure for the BO/BO-bound method is described in Algorithm 1.

To compare the standard BO and BO-bound methods, the mode 1 values reported in [8] were used to fix three of five parameter values as $C = 0.0142$, $n = 0.035$, and $m = 1.47$ along with varying $A \in [50, 350]$ MPa and $B \in [40, 300]$ MPa. The objective of the BO and BO-bound method is to find the $\{A, B\}$ combination that leads to the same forces as measured in the experiment, using the minimum number of objective function simulations. The orthogonal cutting FE simulations were completed using Third Wave Systems' AdvantEdge™. The friction coefficient (for relative sliding between the chip and rake face) was selected as 0.8 [8]. The computation time for each simulation was one hour. For the J-C model, $\dot{\epsilon}_0$ was taken as 1 and T_{ref} was 20 °C.

Two initial LHS samples were used to train the GP model for NMAE followed by 10 iterations. The Matern kernel was used for the GP model with length scale bounds as 0.001 and 100. The

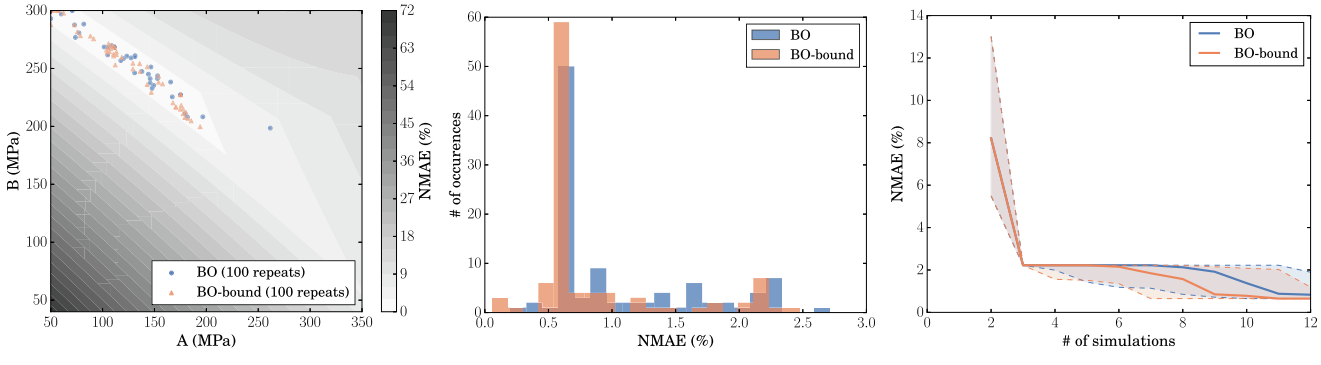

Fig. 1. Comparison of standard BO with BO-bound for the two-dimensional test showing (a) optimal parameters obtained and (b) NMAE histogram after 12 simulations, and (c) convergence of median NMAE w.r.t. number of simulations along with confidence bands representing 25 and 75 percentiles for 100 repeats.

Table 1
Optimal values for the J-C parameters for five repeats of the BO-bound and BO method.

#	Method	A (MPa)	B (MPa)	C	n	m	F_T^{sim} (N)	F_N^{sim} (N)	NMAE (%)
1	BO-bound	202.38	94.97	0.015	0.30	1.21	225.75	94.25	**0.82**
	BO	270.22	77.45	0.043	0.33	1.49	230.46	96.29	2.04
2	BO-bound	272.92	90.74	0.027	0.20	1.13	225.28	94.6	**0.52**
	BO	324.91	183.04	0.037	0.38	1.40	226.60	95.38	0.70
3	BO-bound	220.66	136.85	0.037	0.09	1.21	231.4	95.01	1.67
	BO	105.94	204.34	0.036	0.05	1.48	225.08	94.31	**0.63**
4	BO-bound	279.48	53.48	0.034	0.25	1.27	223.77	93.13	**1.10**
	BO	350.00	40.00	0.005	0.29	1.50	223.05	92.33	1.69
5	BO-bound	292.70	150.63	0.011	0.11	1.09	227.97	93.66	**1.62**
	BO	209.67	201.23	0.012	0.13	1.00	224.56	99.62	2.47

efficiency of any BO method depends on the initial design of experiment (in this case, LHS). To evaluate the robustness of the BO and BO-bound methods Algorithm 1 was repeated 100 times each with a different initial LHS of two samples. To computationally enable completing 100 repeats of BO, each with 12 objective function simulations, a second-order polynomial model was first fitted to the F_T^{sim} and F_N^{sim} as a function of A and B to act as a surrogate for the FE simulations (see Appendix B for details). This enabled rigorously testing the two BO methods without requiring the expensive FE simulation at each iteration.

Fig. 1 shows the results for the 100 repeats of BO and BO-bound completed using the polynomial surrogate model for F_T^{sim} and F_N^{sim}. In Fig. 1(a), each dot represents the best $\{A, B\}$ combination at the end of 12 simulations from the 100 repeats and the contour plot show NMAE from the polynomial surrogate model. BO-bound shows better performance compared to standard BO as seen from the NMAE contour plots in Fig. 1a) and the NMAE convergence plot in Fig. 1(c). From the 100 repeats, 80 cases for the BO-bound method have NMAE less than 1% as compared to 66 for BO as seen from the histogram of NMAE after 12 simulations in Fig. 1(b). In this case, BO-bound takes nine simulations (including the two initial samples) as compared to 11 simulations required by standard BO to reach a median NMAE of less than 1% leading to computational savings of 18% as seen from Fig. 1(c). The confidence bands representing 25 and 75 percentile range from 100 repeats shown in Fig. 1(c) show that BO-bound is more robust than BO. The results show that incorporating the theoretical bounds through the BO-bound method results in improved convergence as compared to the standard BO method.

For the second study, the BO-bound method was tested for calibrating all the five J-C model parameters using the FE simulation in each iteration. The J-C model parameter ranges were selected based on a literature review [8,18–25] to be: $A \in [50, 350]$ MPa, $B \in [40, 220]$ MPa, $C \in [0.001, 0.05]$, $n \in [0.05, 0.5]$, and $m \in [1, 1.5]$. Five initial LHS samples were used to train the GP model for NMAE followed by 20 iterations using BO-bound. The optimal J-C model parameter values were A = 202.38 MPa, B = 77.46 MPa, C = 0.015, n = 0.30, and m = 1.21, with NMAE equal to 0.82%. The sequence of tests and results are shown in Appendix C. Note that the inverse model calibration is done for experimental forces at a single cutting parameter set. The J-C model parameters would not be optimal for cutting forces measured at different cutting parameters. To illustrate, Appendix C shows the simulated and experimental forces at 5° and 25° rake angles using calibrated J-C model parameters at 15° rake angle. For experimental cutting force data at different cutting parameters, an average value of NMAE can be used for the inverse calibration. The process will require running the FE simulations at different cutting parameters in parallel, calculating the NMAE at each (using Eq. 2), and taking the average NMAE value as the output y for the BO-bound method.

To evaluate the robustness of the result, the BO-bound was repeated five times with different initial LHS. For comparison, the standard BO method was also completed for the five repeats. Table 1 shows the best values for the J-C model parameter for each repeat for the BO-bound and BO method. As seen from Table 1, the best NMAE is less than 1.7% for each repeat of BO-bound with a total computational cost of 25 FE simulations in each case. Table 1 also shows that the NMAE is less for BO-bound compared to the standard BO in four out of five repetitions. As noted, the standard BO does not consider the zero bound for NMAE. Table 1 confirms that the inverse calibration of the J-C model parameter from machining forces does not have a unique solution; multiple feasible solutions give force values close to the experimental values [8,18]. Note that even though the flow stress–strain curve for each parameter set is different, they are considered equally valid for the goal of accurately predicting the machining forces.

4. Conclusions

A BO method for calibration of expensive FE simulation models that accounts for known bounds of error functions used as the objective function in inverse model calibration was presented. A case study for inverse calibration of the J-C model parameters was demonstrated. The objective function was the NMAE between the experimental and simulated force components in the tangential and normal directions obtained from an expensive-to-evaluate FE simulation. The proposed BO-bound method considers the non-negativity of the NMAE by suppressing the GP predictions beyond zero through restricting the improvement function values used in the acquisition function of EI. Furthermore, the BO-bound method can generally be applied to any optimization problem with known theoretical bounds on a computationally expensive objective function.

Results on calibrating A and B showed that the BO-bound method converges faster than the standard BO approach and is more robust; BO-bound method led to $\sim 18\%$ computational savings as compared to the standard BO approach for median NMAE from 100 repetitions to reach below 1%. The calibration of all five J-C model parameters showed that the BO-bound method achieves fast convergence with NMAE from each of the five repetitions reaching within 1.7% using only 25 FE simulation and outperforms the standard BO method in four out of five repeats.

Future work will include modifying the BO-bound method to include additional variables (such as cutting temperature and chip thickness), experimental results from different process parameters, and noise in the experimental results. Parallel BO methods [7] will be explored to take advantage of parallelizing the FE simulations in each BO iteration. A multi-objective optimization routine will also be evaluated where the error in each force prediction is modeled separately to determine the optimal FE model parameters.

Declaration of Competing Interest

The authors declare that they have no known competing financial interests or personal relationships that could have appeared to influence the work reported in this paper.

Acknowledgements

This work has been supported in part by the DOE Office of Energy Efficiency and Renewable Energy (EERE), Manufacturing Science Division, and used resources at the Manufacturing Demonstration Facility, a DOE-EERE User Facility at Oak Ridge National Laboratory. The second author acknowledges support from Department of Energy award number DE-SC0021239.

The authors would also like to thank Dr. Patxi Fernandez-Zelaia, Oak Ridge National Laboratory, for sharing the experimental data used in the paper.

Appendix A. Expected improvement acquisition function

In this section, the EI acquisition function used in the standard BO is described in A.1 followed by the derivation of EI for BO-bound in A.2. An illustrative example is provided in Example 1 to further explain BO and BO-bound acquisition functions.

A.1. Derivation of EI for standard BO

Let $y^k_{\min} = \min\{y^{(1)}, \ldots, y^{(k)}\}$ be the current best function value after k simulations, where $\{y^{(1)}, \ldots, y^{(k)}\}$ are observations at $\{\mathbf{x}_1, \ldots, \mathbf{x}_k\}$, respectively. The GP prediction at any $\mathbf{x}$ is a normal distribution with the mean $\mu(\mathbf{x})$ and the standard deviation $\sigma(\mathbf{x})$. The improvement function $I(\mathbf{x})$ for a minimization problem is given by Eq. (3). The probability of improvement when $\mathscr{Y}(\mathbf{x}) \leqslant y^k_{\min}$ is $P_I(\mathbf{x}) = \mathbb{P}\left[\mathscr{Y}(\mathbf{x}) \leqslant y^k_{\min}\right] = \Phi(\beta(\mathbf{x}))$,where $\beta(\mathbf{x}) = (y^k_{\min} - \mu(\mathbf{x}))/\sigma(\mathbf{x})$. The EI is given by

$$\begin{aligned}\mathbb{E}[I(\mathbf{x})] &= P_I(\mathbf{x})\mathbb{E}\left[y^k_{\min} - \mathscr{Y}(\mathbf{x}) \mid \mathscr{Y}(\mathbf{x}) \leqslant y^k_{\min}\right] \\ &\quad + (1 - P_I(\mathbf{x})) \times 0 = P_I(\mathbf{x})\left(y^k_{\min} - \mathbb{E}\left[\mathscr{Y}(\mathbf{x}) \mid \mathscr{Y}(\mathbf{x}) \leqslant y^k_{\min}\right]\right) \\ &= \Phi(\beta(\mathbf{x}))\left(y^k_{\min} - \left(\mu(\mathbf{x}) - \sigma(\mathbf{x})\frac{\phi(\beta(\mathbf{x}))}{\Phi(\beta(\mathbf{x}))}\right)\right) \\ &= (y^k_{\min} - \mu(\mathbf{x}))\Phi(\beta(\mathbf{x})) + \sigma(\mathbf{x})\phi(\beta(\mathbf{x})),\end{aligned} \tag{7}$$

A.2. Derivation of EI for BO-bound with bounded objective functions

The modified improvement function $I_B(\mathbf{x})$ is given by Eq. (5), which restricts the maximum improvement to $y^k_{\min}$ when $\mathscr{Y}(\mathbf{x}) \leqslant 0$ since NMAE has a lower bound of 0. The probability of improvement when $\mathscr{Y}(\mathbf{x}) \leqslant 0$ is

$$P_{I_1}(\mathbf{x}) = \mathbb{P}[\mathscr{Y}(\mathbf{x}) \leqslant 0] = \Phi(\alpha(\mathbf{x})), \tag{8}$$

where $\alpha(\mathbf{x}) = (0 - \mu(\mathbf{x}))/\sigma(\mathbf{x})$. The probability of lying within $0 < \mathscr{Y}(\mathbf{x}) \leqslant y^k_{\min}$ is

$$P_{I_2}(\mathbf{x}) = \mathbb{P}\left[0 < \mathscr{Y}(\mathbf{x}) \leqslant y^k_{\min}\right] = \Phi(\beta(\mathbf{x})) - \Phi(\alpha(\mathbf{x})). \tag{9}$$

The EI for bounded improvement function in BO-bound is given by

$$\begin{aligned}\mathbb{E}\ [I_B(\mathbf{x})] &= P_{I_1}(\mathbf{x})\mathbb{E}\left[y^k_{\min} \mid \mathscr{Y}(\mathbf{x}) \leqslant 0\right] + P_{I_2}(\mathbf{x})\mathbb{E}\left[y^k_{\min} - \mathscr{Y}(\mathbf{x}) \mid 0 < \mathscr{Y}(\mathbf{x}) \leqslant y^k_{\min}\right] + \left(1 - P_{I_1}(\mathbf{x}) - P_{I_2}(\mathbf{x})\right) \times 0 \\ &= P_{I_1}(\mathbf{x})y^k_{\min} + P_{I_2}(\mathbf{x})\left(y^k_{\min} - \mathbb{E}\left[\mathscr{Y}(\mathbf{x}) \mid 0 < \mathscr{Y}(\mathbf{x}) \leqslant y^k_{\min}\right]\right) \\ &= \Phi(\alpha(\mathbf{x}))y^k_{\min} + (\Phi(\beta(\mathbf{x})) - \Phi(\alpha(\mathbf{x})))\left(y^k_{\min} - \left(\mu(\mathbf{x}) - \sigma(\mathbf{x})\left(\frac{\phi(\beta(\mathbf{x})) - \phi(\alpha(\mathbf{x}))}{\Phi(\beta(\mathbf{x})) - \Phi(\alpha(\mathbf{x}))}\right)\right)\right) \\ &= \Phi(\alpha(\mathbf{x}))y^k_{\min} + (y^k_{\min} - \mu(\mathbf{x}))(\Phi(\beta(\mathbf{x})) - \Phi(\alpha(\mathbf{x}))) + \sigma(\mathbf{x})(\phi(\beta(\mathbf{x})) - \phi(\alpha(\mathbf{x}))).\end{aligned} \tag{10}$$

Example 1 (*Illustrative example showing BO and BO-bound EI*). Let the true function be $y(x) = (6x-2)^2\sin(12x-4) - 6.02$ with a known lower bound of zero (global minimum is zero at $x = 0.76$). Fig. A.2(a) shows the GP fit using four training data at $\{x_i\}_{i=1}^4 = \{0, 0.45, 0.65, 1\}$ with corresponding observations $\{y^{(i)}\}_{i=1}^4 = \{9.04, 6.50, 3.81, 21.85\}$. Based on the current y obser-

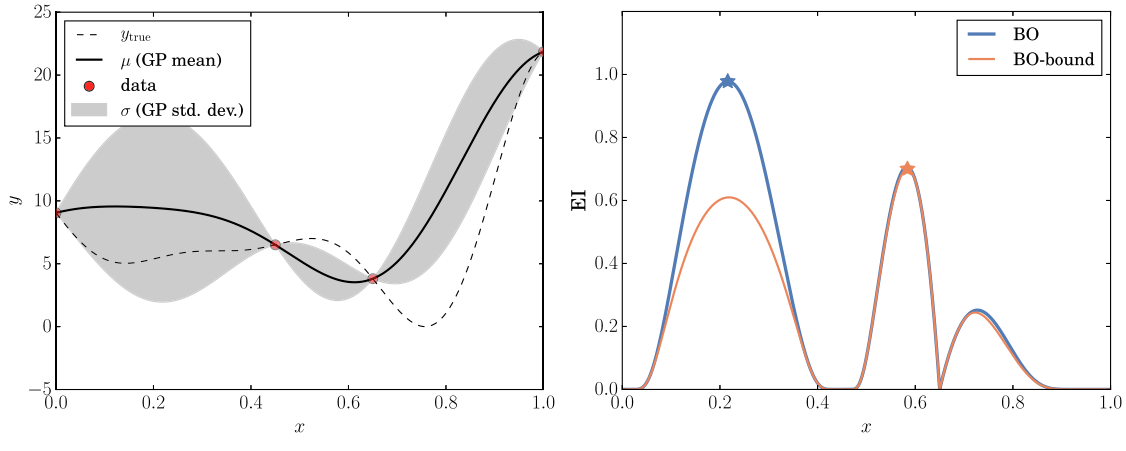

(a) (b)

Fig. A.2. Illustrative example showing (a) GP surrogate fit with true objective function y_{true} and (b) EI for BO and BO-bound with the maximum locations marked with a star.

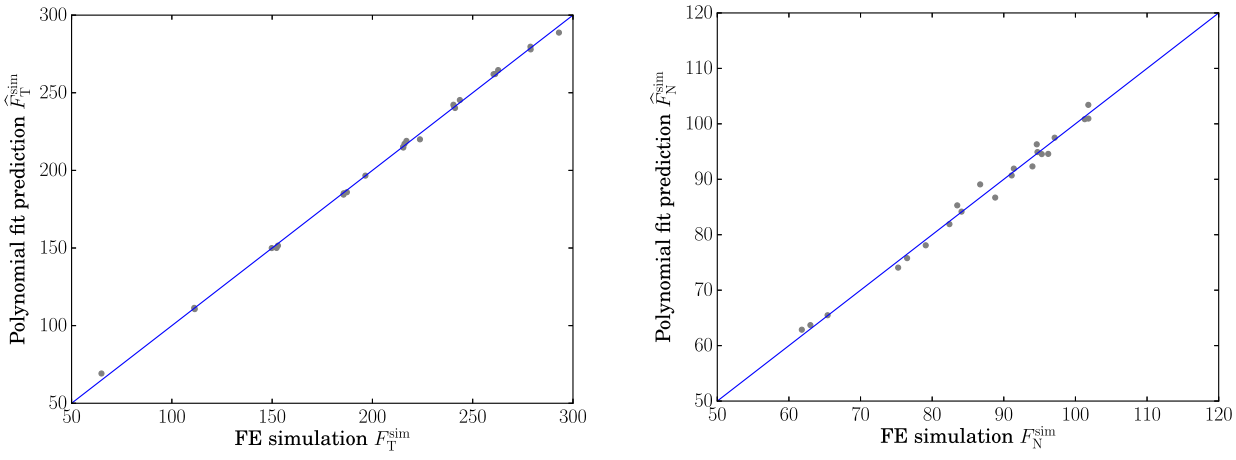

(a) (b)

Fig. B.3. Leave one out cross-validation plot for the second-order polynomial model for predicting (a) F_T^{sim} and (b) F_N^{sim}.

vations, the best function value is $y_{min} = 3.81$ at $x = 0.65$. Fig. A.2 (b) shows the EI in y_{min} as a function of x for BO and BO-bound and can be seen to be different. The maximum value of EI is marked with a star for BO and BO-bound in Fig. A.2(b)(b) to show the difference in the next sample selection. The maximum EI is equal to 0.98 and occurs at $x = 0.22$ for standard BO while the maximum EI is equal to 0.7 and occurs at $x = 0.58$ for BO-bound. The BO-bound method penalizes the negative prediction values at $x = 0.22$ and restricts the maximum improvement for $I_B(x)$ to $y_{min} = 3.81$; this reduces the EI for BO-bound at $x = 0.22$ and switches the maximum location to $x = 0.58$.

Appendix B. Second-order polynomial fit for algorithm testing

In this work, 25 FE simulations were completed using an equally-spaced 5×5 grid and the force values for each sample were recorded. A second-order polynomial fit to this data was used as the FE surrogate in BO to eliminate the need to complete expensive FE simulations at each BO iteration in the first study to rigorously analyze the BO approaches. Fig. B.3 shows the leave-one-out cross-validation results for the surrogate model. The polynomial surrogate model for F_T^{sim} and F_N^{sim} are

Table C.2
NMAE values for J-C model parameter simulations using BO-bound for one repetition.

#	A (MPa)	B (MPa)	C	n	m	F_T^{sim} (N)	F_N^{sim} (N)	NMAE (%)
1	270.23	77.46	0.043	0.33	1.49	271.91	110.90	18.97
2	195.15	101.69	0.014	0.31	1.20	230.46	96.29	2.04
3	75.02	179.63	0.036	0.08	1.01	181.00	75.70	19.82
4	115.54	298.35	0.023	0.47	1.32	596.84	242.34	160.58
5	338.04	217.70	0.001	0.18	1.15	281.61	120.64	26.26
6	192.36	104.21	0.014	0.31	1.20	235.42	96.47	3.25
7	**202.38**	**94.97**	**0.015**	**0.30**	**1.21**	**225.75**	**94.25**	**0.82**
8	194.82	94.12	0.016	0.29	1.21	221.10	92.30	2.14
9	209.22	96.31	0.014	0.31	1.22	232.60	96.80	2.79
10	194.34	89.04	0.015	0.31	1.22	217.66	90.79	3.70
11	205.60	99.29	0.015	0.30	1.21	229.74	95.46	1.45
12	201.00	93.58	0.014	0.29	1.20	219.75	91.43	2.90
13	201.18	100.40	0.016	0.30	1.22	230.55	95.49	1.64
14	350.00	40.00	0.050	0.05	1.50	253.39	88.71	9.89
15	190.18	40.00	0.050	0.05	1.50	179.40	71.70	22.28
16	350.00	40.00	0.024	0.05	1.50	228.91	83.81	7.01
17	350.00	40.00	0.032	0.050	1.320	226.96	80.89	8.11
18	350.00	79.27	0.031	0.050	1.465	249.40	88.50	9.11
19	350.00	45.69	0.005	0.050	1.385	205.98	78.34	12.85
20	350.00	40.12	0.032	0.127	1.482	241.89	92.00	5.60
21	350.00	65.74	0.020	0.152	1.500	246.82	98.93	7.08
22	350.00	40.00	0.032	0.316	1.500	254.59	103.47	11.20
23	306.36	40.00	0.024	0.109	1.500	217.33	85.88	6.36
24	350.00	40.00	0.020	0.203	1.500	235.00	95.42	2.60
25	342.64	40.00	0.010	0.251	1.500	224.66	93.74	0.84

Table C.3
Using the calibrated J-C model parameters at different rake angles.

	Rake angle (°)	F_T^{expt} (N)	F_N^{expt} (N)	F_T^{sim} (N)	F_N^{sim} (N)	NMAE (%)
Calibration	15	224.1	95.1	225.75	94.25	0.82
Test	5	261.2	171.3	289.7	178.3	7.49
Test	25	178.5	43.3	170.1	43.1	2.69

$$\widehat{F}_{\mathrm{T}}^{\mathrm{sim}} = 2.98339 + 0.698A + 0.811B - 0.000374A^2 - 0.000470B^2 - 0.001083AB$$
$$\widehat{F}_{\mathrm{N}}^{\mathrm{sim}} = -3.2744 + 0.354A + 0.384B - 0.000356A^2 - 0.000253B^2 - 0.000715AB$$

Appendix C. Sequence of simulations for the BO-bound method

Table C.2 shows the results with the first five rows showing the initial LHS samples followed by 20 subsequent simulations determined by the BO-bound method. The optimal J-C model parameters are highlighted in bold. The NMAE for the optimal J-C model parameters after 25 simulation was 0.82%.

Table C.3 shows the simulated and experimental forces at 5° and 25° rake angles using calibrated J-C model parameters at 15° rake angle.

References

[1] Melkote SN, Grzesik W, Outeiro J, Rech J, Schulze V, Attia H, Arrazola P-J, M'Saoubi R, Saldana C. Advances in material and friction data for modelling of metal machining. Cirp Annals 2017;66(2):731–54.
[2] Bariani P, Dal Negro T, Bruschi S. Testing and modelling of material response to deformation in bulk metal forming. CIRP Annals 2004;53 (2):573–95.
[3] Willcox KE, Ghattas O, Heimbach P. The imperative of physics-based modeling and inverse theory in computational science. Nature Comput Sci 2021;1 (3):166–8.
[4] Jones DR, Schonlau M, Welch WJ. Efficient global optimization of expensive black-box functions. J Global Optimiz 1998;13(4):455–92.
[5] Frazier PI. Bayesian optimization. In: Recent Advances in Optimization and Modeling of Contemporary Problems, INFORMS; 2018. p. 255–278..
[6] Forrester A, Sobester A, Keane A. Engineering design via surrogate modelling: a practical guide. John Wiley & Sons; 2008.
[7] Haftka RT, Villanueva D, Chaudhuri A. Parallel surrogate-assisted global optimization with expensive functions–a survey. Struct Multidisc Optimiz 2016;54(1):3–13.
[8] Fernandez-Zelaia P, Melkote SN. Statistical calibration and uncertainty quantification of complex machining computer models. Int J Mach Tools Manuf 2019;136:45–61.
[9] Arrazola P, Özel T, Umbrello D, Davies M, Jawahir I. Recent advances in modelling of metal machining processes. Cirp Annals 2013;62(2):695–718.
[10] Zhou T, Wu J, Che J, Wang Y, Wang X. Dynamic shear characteristics of titanium alloy ti-6al-4v at large strain rates by the split hopkinson pressure bar test. Int J Impact Eng 2017;109:167–77.
[11] Chandrasekaran H, M'saoubi R, Chazal H. Modelling of material flow stress in chip formation process from orthogonal milling and split hopkinson bar tests. Mach Sci Technol 2005;9(1):131–45.
[12] Shrot A, Bäker M. Determination of johnson–cook parameters from machining simulations. Comput Mater Sci 2012;52(1):298–304.
[13] Germain G, Morel A, Braham-Bouchnak T. Identification of material constitutive laws representative of machining conditions for two titanium alloys: Ti6al4v and ti555-3, J Eng Mater Technol 135 (3)..
[14] Malakizadi A, Cedergren S, Sadik I, Nyborg L. Inverse identification of flow stress in metal cutting process using response surface methodology. Simul Model Pract Theory 2016;60:40–53.
[15] Özel T, Karpat Y. Identification of constitutive material model parameters for high-strain rate metal cutting conditions using evolutionary computational algorithms. Mater Manuf Processes 2007;22(5):659–67.
[16] Chen G, Ren C, Yu W, Yang X, Zhang L. Application of genetic algorithms for optimizing the johnson–cook constitutive model parameters when simulating the titanium alloy ti-6al-4v machining process. Proc Inst Mech Eng, Part B: J Eng Manuf 2012;226(8):1287–97.
[17] Crichigno Filho J. Applying extended oxley's machining theory and particle swarm optimization to model machining forces. Int J Adv Manuf Technol 2017;89(1–4):1127–36.
[18] Lesuer DR, Kay G, LeBlanc M. Modeling large-strain, high-rate deformation in metals, Tech. rep., Lawrence Livermore National Lab., CA (US); 2001..
[19] Adibi-Sedeh AH, Madhavan V, Bahr B. Extension of oxley's analysis of machining to use different material models. J Manuf Sci Eng 2003;125(4):656–66.
[20] Daoud M, Jomaa W, Chatelain J, Bouzid A. A machining-based methodology to identify material constitutive law for finite element simulation. Int J Adv Manuf Technol 2015;77(9–12):2019–33.
[21] Dabboussi W, Nemes J. Modeling of ductile fracture using the dynamic punch test. Int J Mech Sci 2005;47(8):1282–99.
[22] Guo Y. An integral method to determine the mechanical behavior of materials in metal cutting. J Mater Process Technol 2003;142(1):72–81.
[23] Rule WK. A numerical scheme for extracting strength model coefficients from taylor test data. Int J Impact Eng 1997;19(9–10):797–810.
[24] Manes A, Peroni L, Scapin M, Giglio M. Analysis of strain rate behavior of an al 6061 t6 alloy. Procedia Eng 2011;10:3477–82.
[25] Fish J, Oskay C, Fan R, Barsoum R. Al 6061-t6-elastomer impact simulations, Electronic document..